International Journal of analytical and Numerical Methods in Mechanical Design
Vol 2., Issue 2, Summer & Autumn 2023, 23-36

Nonlinear buckling analysis of different types of porous FG cylindrical sandwich shells

Mohsen Rahmani [a*], Younes Mohammadi [b], Mahdi Abtahi [b]

[a] Department of Mechanics, Tuyserkan Branch, Islamic Azad University, Tuyserkan, Iran
[b] Department of Mechanical Engineering, Qazvin Branch, Islamic Azad University, Qazvin, Iran

Received 19 April 2024, Accepted 30 January 2025

Abstract

Based on a modified higher order sandwich shell theory, the buckling behaviours of cylindrical sandwich shells are investigated. Sandwiches consist of two functionally graded face-sheets and a homogenous core in type-I and two homogeneous face-sheets and a functionally graded core in type-II. Functionally graded materials are varied gradually across the thickness based on a power law rule which modified by considering the even and uneven porosity distributions. All materials are temperature dependent. Nonlinear Von-Karman strain, thermal stresses in all layers and in-plane strain and transverse flexibility of the core are considered to obtain the governing equations based on the minimum potential energy principle. A Galerkin method is used to solve in simply supported and clamped boundary conditions under an axial in-plane compressive load. The results of the present method are compared with some literatures to verify the procedure. Also, the effect of variation of temperature, some geometrical parameters and porosities on the critical load are studied.

Keywords: Porosity, Temperature-dependent, FGM, Buckling, Boundary condition, Sandwich shell

1. Introduction

High performance and high bending rigidity with a low weight make the modern industries such as nuclear reactor, aerospace, marine, satellite, aircraft, sport devices and construction to use the sandwich structures which usually composed of two thin and stiff face sheets that cover a thick and soft core. To avoid the delamination, stress concentration and failure in the ordinary composite materials and laminates in the sandwich panels in high temperature conditions, functionally graded materials have been proposed by Japanese scientists which are in-homogeneous microscopic materials and their properties vary across the thickness smoothly. But during the manufacturing the FGMs, some micro voids are appeared that affect the materials properties, so the porosity distributions should be considered to modify the models of FGMs. Also, the high temperature conditions affect the material properties, so it is important to consider the dependency of materials properties to the temperature (Rahmani, Mohammadi et al. 2019, Rahmani, Mohammadi et al. 2020).

In the classical plate and shell theories, the core is considered as an inflexible layer, but to accurate investigation of the mechanical behavior of sandwich structures and detect some local modes, the core should be considered as a transversely flexible layer. So, the high order sandwich theory was presented (Frostig, Baruch et al. 1992). Many researchers have been studied the mechanical behaviors of cylindrical sandwich shells such as buckling and post-buckling by using different theories. Lopatin and Morozov presented the buckling analysis of fully clamped composite sandwich cylindrical shell subjected to uniform lateral pressure by using the Galerkin method (Lopatin and Morozov 2015). Shahgholian and Rahimi investigated the global buckling of composite cylindrical shells with lattice cores under uniaxial compression based on the smeared stiffener method and using Rayleigh-Ritz method (Ghahfarokhi and Rahimi 2018). Hieu et al. studied the buckling and postbuckling behavior of FGM sandwich cylindrical shells subjected to external pressure in thermal conditions based on the classical shell theory and using Galerkin method (Hieu and Tung 2021). Daikh studied the thermal buckling of FG sandwich cylindrical shell based on the Donnell theory. Material properties was modelled by sigmoid function and the thermal uniform, linear and nonlinear loads distributions were considered (Eslami, Eslami et al. 2018).Based on the Donnell shell theory and smeared technique, Nam et al. studied the nonlinear torsional buckling and postbuckling of sandwich FG cylindrical shells reinforced by stiffeners under thermal conditions (Nam, Phuong et al. 2019). Fallah and Taati studied the nonlinear bending and post-buckling of laminated sandwich cylindrical shells with isotropic, FG or isogrid core under the thermo-mechanical loadings and different boundary conditions (Fallah and Taati 2019). Balbin and Bisagni studied the buckling of sandwich cylindrical shells with composite face sheets and a deformable core (Balbin and Bisagni 2021). Based on the Donnell shell theory, Chan et al. studied the nonlinear buckling and postbuckling of imperfect FG porous sandwich cylindrical panels subjected to axial loading under various boundary conditions (Chan, Van Hoan et al.

*Corresponding author Email address: mohsen_rahmani@ymail.com

2021). Hung et al. studied the nonlinear buckling and post buckling of spiral corrugated sandwich FG cylindrical shells under external pressure resting on the elastic foundation and based on the Donnell shell theory and using a Galerkin method to solve the problems (Tho Hung, Thuy Dong et al. 2020). Semenyuk et al. investigated the stability and initial post-buckling behavior of orthotropic cylindrical sandwich shells by asymptotic Koiter–Budiansky method (Semenyuk, Trach et al. 2019). Malekzadeh et al. studied the free vibration and buckling analysis of cylindrical sandwich panel with magneto rheological layer based on an improved higher order sandwich panel theory (MalekzadehFard, Gholami et al. 2017). Shatov et al. studied the buckling of sandwich cylindrical shell with composite lattice core under hydrostatic pressure based on a finite element method (Shatov, Burov et al. 2020). Nam et al. investigated the nonlinear buckling and post-buckling of FG porous circular cylindrical shells reinforced by orthogonal stiffeners resting on elastic foundation in thermal condition and under torsional load by using the classical shell theory (Nam and Trung 2019). Phuong et al. investigated the nonlinear stability of FG sandwich cylindrical shells with stiffeners under axial compression in thermal conditions based on the Donnell shell theory (Phuong, Nam et al. 2019). Han et al. studied the buckling behavior of cylinder shell with FGM coating under the thermal (Han, Wang et al. 2017). Evkin presented mathematical model of local buckling of cylindrical shells based on Pogorelov's geometrical method (Evkin 2019). Trablesi et al. studied the thermal buckling of FG plates and cylindrical shells by usisng a modified first order shear deformation theory (Trabelsi, Frikha et al. 2019). Mehralian and Beni studied the size-dependent torsional buckling behavior of FG cylindrical shell based on modified couple stress theory using shell model and GDQ method (Mehralian and Beni 2016). Fan studied the critical buckling load of compresses cylindrical shell based on the non-destructive probing method (Fan 2019). Sofiyev and Hui studied the vibration and stability of FG cylindrical shells under the external pressure based on the first order shear deformation theory and Galerkin method (Sofiyev and Hui 2019). Based on the Donnell shell theory, Gao et al. studied the dynamic stability behavior of FG orthotropic cylindrical shell resting on the elastic foundation (Gao, Gao et al. 2018). Sheng and Wang studied the dynamic stability and nonlinear vibration of stiffened FG cylindrical shell in thermal condition by using FSDT, smearing method and Bolotin method (Sheng and Wang 2018). Sofiyev et al. studied the effect of shear stresses and rotary inertia on the stability and vibration of sandwich cylindrical shells with FG core resting on the elastic medium based on the FSDT (Sofiyev, Hui et al. 2016). Asai et al. investigated the thermal instability of geometrically imperfect sandwich cylindrical shells under uniform heating based on the Brinson phenomenological model and third order shear deformation theory. The sandwich were made of FG face sheets and a SMA fiber reinforced composite core (Asadi, Akbarzadeh et al. 2015).

By reviewing the accessible references, it's found that more investigation should be done in the critical load responses. To study the buckling behavior of two kinds of sandwich cylindrical shells in the uniform temperature distributions under the clamped and simply supported boundary conditions, a modified high order sandwich shell theory is used to detect the more accurate modes. In sandwich type-I, a homogeneous core is covered by FG face sheets, and in sandwich type-II, two homogeneous face sheets coat a FG core. A power law rule which modified by considering the even and uneven porosity distributions are used to model the gradually variation of the FGMs. Also, all materials are considered temperature dependent. In-plane stresses and high order stresses of the core, and thermal stresses and thermal stress resultants of the face-sheets and core, which usually ignored by the researchers, are considered in this paper. The equations are derived based on the minimum potential energy principle under an axial compression and nonlinear Von-Karman strains are used. A Galerkin method is used to solve the equations. The effects of the temperature variation, some geometrical parameters and porosity variation on the critical load of sandwich beams are investigated, too.

2. Formulation

Consider two types of sandwich cylindrical shells which are shown in Fig.1. In sandwich type-I, a homogeneous core is covered by two porous FG face sheets, and in sandwich type-II the homogeneous face sheets cover a porous FG core.

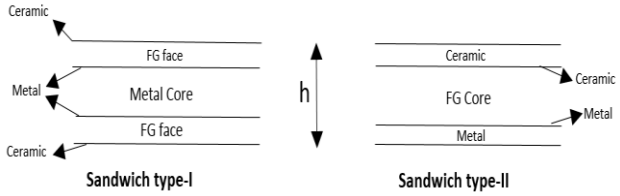

Fig .1. Schematic of various models of sandwich cylindrical shell

All materials are temperature dependent which modelled as follows (Rahmani, Mohammadi et al. 2020):

$$P = P_0\left(P_{-1}T^{-1} + 1 + P_1T + P_2T^2 + P_3T^3\right) \tag{1}$$

where "P"s are coefficients of temperature, and they are unique for each material; $T=T_0+\Delta T$, which T_0 is equal to 300(K). A power law rule which consists of even porosity volume fraction is presented to model the FGM properties for type-I as follow (Rahmani, Mohammadi et al. 2020):

$$P_j\left(z_j,T\right) = g\left(z_j\right)P_{ce}^j(T) + \left[1-g\left(z_j\right)\right]P_m^j(T) - (P_{ce}^j(T)+P_m^j(T))\frac{\zeta}{2};\quad j=(o,i) \tag{2}$$

$$g\left(z_o\right) = \left(\frac{\frac{h_o}{2}-z_o}{h_o}\right)^N;\quad g\left(z_i\right) = \left(\frac{\frac{h_i}{2}+z_i}{h_i}\right)^N; \tag{3}$$

And the materials properties equation for sandwich type-II is as follows (Rahmani, Mohammadi et al. 2020):

$$P_c(z_c,T)=g(z_c)P_{ce}^c(T)+ \quad (4)$$
$$\left[1-g(z_c)\right]P_m^c(T)-(P_{ce}^c(T)+P_m^c(T))\frac{\zeta}{2}$$

$$g(z_c)=(\frac{\frac{h_c}{2}-z_c}{h_c})^N \quad (5)$$

where "N" is the constant power law index; g(z) and [1-g(z)] are volume fraction of ceramic and metal; "ζ" is the porosity distribution; and subscripts "o", "i" and "c" refer to outer and inner faces and the core, respectively. In the uneven case, the micro voids are spread in the middle area of the layers and decrease near to the edges and tend to the zero. So, power law rule in the uneven case for the type-I is modified as follows (Rahmani, Mohammadi et al. 2020):

$$P_j(z_j,T)=g(z_j)P_{ce}^j(T)+\left[1-g(z_j)\right]P_m^j(T)- \quad (6)$$
$$(P_{ce}^j(T)+P_m^j(T))\frac{\zeta}{2}(1-\frac{2|z|}{h}),\ j=(t,b)$$

And for In the type-II it is presented as follows (Rahmani, Mohammadi et al. 2020):

$$P_c(z_c,T)=g(z_c)P_{ce}^c(T)+\left[1-g(z_c)\right]P_m^c(T)- \quad (7)$$
$$(P_{ce}^c(T)+P_m^c(T))\frac{\zeta}{2}(1-\frac{2|z_c|}{h})$$

The minimum potential energy principle is used to obtain the governing equations of sandwich cylindrical shells which include potential of the external loads, "V", and total strain energy, "U"; This principle is presented as follows (Rahmani, Mohammadi et al. 2019):

$$\prod(\delta U+\delta V)=0 \quad (8)$$

which "δ" denotes the variation operator. The variation of the total strain energy includes mechanical stresses and thermal stresses with nonlinear strains in the faces and core. The compatibility conditions rule as constraints which are attended as six Lagrange multipliers in the principle. By considering the in-plane stresses of the core, "δU" is as follows:

$$\delta U=\int_{V_o}(\sigma_{ss}^o\delta\varepsilon_{ss}^o+\sigma_s^{oT}\delta d_{ss}^o+\sigma_{\theta\theta}^o\delta\varepsilon_{\theta\theta}^o+\sigma_{\theta\theta}^{oT}\delta d_{\theta\theta}^o+\tau_{s\theta}^o\delta\gamma_{s\theta}^o+ \quad (9)$$
$$\tau_{sz}^o\delta\gamma_{sz}^o+\tau_{\theta z}^o\delta\gamma_{\theta z}^o)dV_o+\int_{V_i}(\sigma_{ss}^i\delta\varepsilon_{ss}^i+\sigma_s^{iT}\delta d_{ss}^i+\sigma_{\theta\theta}^i\delta\varepsilon_{\theta\theta}^i+$$
$$\sigma_{\theta\theta}^{iT}\delta d_{\theta\theta}^i+\tau_{s\theta}^i\delta\gamma_{s\theta}^i+\tau_{sz}^i\delta\gamma_{sz}^i+\tau_{\theta z}^i\delta\gamma_{\theta z}^i)dV_i+\int_{V_c}(\sigma_{ss}^c\delta\varepsilon_{ss}^c+$$
$$\sigma_s^{iT}\delta d_{ss}^i+\sigma_{\theta\theta}^c\delta\varepsilon_{\theta\theta}^c+\sigma_{\theta\theta}^{cT}\delta d_{\theta\theta}^c+\sigma_{zz}^c\delta\varepsilon_{zz}^c+\sigma_{zz}^{cT}\delta d_{zz}^c+\tau_{s\theta}^c\delta\gamma_{s\theta}^c$$
$$+\tau_{sz}^c\delta\gamma_{sz}^c+\tau_{\theta z}^c\delta\gamma_{\theta z}^c)dV_c$$
$$+\delta\int_0^L\int_0^{2\pi}[\lambda_{so}\left(u_o(z_o=h_o/2)-u_c(z_c=-h_c/2)\right)$$
$$+\lambda_{\theta o}\left(v_o(z_o=h_o/2)-v_c(z_c=-h_c/2)\right)$$
$$+\lambda_{zo}\left(w_o(z_o=h_o/2)-w_c(z_c=-h_c/2)\right)$$
$$+\lambda_{si}\left(u_c(z_c=h_c/2)-u_i(z_i=-h_i/2)\right)$$
$$+\lambda_{\theta i}\left(v_c(z_c=h_c/2)-v_i(z_i=-h_i/2)\right)$$
$$+\lambda_{zi}\left(w_c(z_c=h_c/2)-w_i\right)]rdsd\theta$$

where σ_{ss}, $\sigma_{\theta\theta}$ and $\tau_{s\theta}$ display the in-plane normal and shear stresses; ε_{ss}, $\varepsilon_{\theta\theta}$ and $\gamma_{s\theta}$ are the in plane normal and shear strains of the layers; $\sigma^T{}_{ss}$ and $\sigma^T{}_{\theta\theta}$ express the thermal stresses; $\sigma^c{}_{zz}$ and $\varepsilon^c{}_{zz}$ present the lateral normal stress and strain in the core; $\tau^c{}_{sz}$, $\tau^c{}_{\theta z}$, $\gamma^c{}_{sz}$ and $\gamma^c{}_{\theta z}$ declare shear stresses and shear strains in the core; and λ_s, λ_θ and λ_z are the Lagrange multipliers at the face sheet-core interfaces. It should be noted that the material properties in the functionally graded layers are the function of the displacement and the temperature, and in the homogeneous layers are just function of the temperature

The variation of the external loads as follows (Rahmani and Dehghanpour 2020):

$$\delta V= \quad (10)$$
$$-\int_0^L\int_0^{2\pi}(P_o\delta w_{0o}+P_i\delta w_{0i}+n_s^o\delta u_{0o}+n_s^i\delta u_{0i})r\,d\theta ds$$

where "u_0^j" and w_0^j(j = o, i) are the displacements of the mid-plane of the face sheets in the longitudinal and vertical directions, respectively; "n_s^j" are the in-plane external loads of the top and bottom face sheets; and, "P_o" and "P_i" are the vertical distributed loads applied on the top and bottom face sheets, respectively.

The displacement fields of the face sheets are modelled by the first order shear deformation theory.

$$u_j(s,\theta,z_j)=u_{0j}(s,\theta)+z_j\phi_s^j(s,\theta);\ j=(o,i) \quad (11)$$
$$v_j(s,\theta,z_j)=v_{0j}(s,\theta)+z_j\phi_\theta^j(s,\theta) \quad (12)$$
$$w_j(s,\theta,z_j)=w_{0j}(s,\theta) \quad (13)$$

where subscript "0" expresses values in association with the middle surface of the layers; and "ϕ" is the rotation of the normal to the middle surface. The kinematic relations of the core are presented as cubic patterns which contain seven unknown coefficients as follows:

$$u_c(s,\theta,z_c)=u_0(s,\theta)+u_1(s,\theta)z_c+ \quad (14)$$
$$u_2(s,\theta){z_c}^2+u_3(s,\theta){z_c}^3$$

$$v_c(s,\theta,z_c)=v_0(s,\theta)+v_1(s,\theta)z_c+ \quad (15)$$
$$v_2(s,\theta){z_c}^2+v_3(s,\theta){z_c}^3$$

$$w_c(s,\theta,z_c)=w_0(s,\theta)+w_1(s,\theta)z_c+ \quad (16)$$
$$w_2(s,\theta){z_c}^2$$

The nonlinear von Kármán strain-displacement relations for the face sheets (j=o, i) can be defined as (Rahmani, Mohammadi et al. 2019, Rahmani, Mohammadi et al. 2020):

$$\varepsilon_{ss}^{j}=u_{0j,s}+z_j\varphi_{s,s}^{j}+\frac{1}{2}{w_{j,s}}^2-\alpha_j\Delta T_j \quad (17)$$

$$\varepsilon_{\theta\theta}^{j}=\frac{1}{r}\left(v_{0j,\theta}+z_j\varphi_{\theta,\theta}^{j}+w_j\right)+\frac{1}{2r^2}{w_{j,\theta}}^2-\alpha_j\Delta T_j \quad (18)$$

$$\varepsilon_{zz}^{j}=-\alpha_j\Delta T_j \quad (19)$$

$$\gamma_{s\theta}^{j}=\frac{1}{r}\left(u_{0j,\theta}+z_j\varphi_{s,\theta}^{j}\right)+v_{0j,s}+z_j\varphi_{\theta,s}^{j}+\frac{1}{r}w_{j,s}w_{j,\theta} \quad (20)$$

$$\gamma_{sz}^{j}=\varphi_s^{j}+w_{j,s} \quad (21)$$

$$\gamma_{\theta z}^{j}=\frac{1}{r}\left(w_{j,\theta}-v_{0j}-z_j\varphi_\theta^{j}\right)+\varphi_\theta^{j} \quad (22)$$

The"(),i" expresses derivation with respect to "i". The strain of the core can be defined as:

$$\varepsilon_{ss}^{c}=u_{0,s}+u_{1,s}z_c+u_{2,s}{z_c}^2+u_{3,s}{z_c}^3+ \quad (23)$$
$$\frac{1}{2}{w_{0,s}}^2-\alpha_c\Delta T_c$$

$$\varepsilon_{\theta\theta}^{c}= \quad (24)$$
$$\frac{1}{r}\left[v_{0,\theta}+v_{1,\theta}z_c+v_{2,\theta}{z_c}^2+v_{3,\theta}{z_c}^3+\left(w_0+w_1z_c+w_2{z_c}^2\right)\right]$$
$$+\frac{1}{2r^2}{w_{0,\theta}}^2-\alpha_c\Delta T_c$$

$$\varepsilon_{zz}^{c}=w_1+2w_2z_c-\alpha_c\Delta T_c \quad (25)$$

$$\gamma_{sz}^{c}=\left(u_1+2u_2z_c+3u_3{z_c}^2\right)+ \quad (26)$$
$$\left(w_{0,s}+w_{1,s}z_c+w_{2,s}{z_c}^2\right)$$

$$\gamma_{\theta z}^{c}= \quad (27)$$
$$\frac{1}{r}\left[w_{0,\theta}+w_{1,\theta}z_c+w_{2,\theta}{z_c}^2-\left(v_0+v_1z_c+v_2{z_c}^2+v_3{z_c}^3\right)\right]$$
$$+v_1+2v_2z_c+3v_3{z_c}^2$$

$$\gamma_{s\theta}^{c}= \quad (28)$$
$$\frac{1}{r}\left[u_{0,\theta}+u_{1,\theta}z_c+u_{2,\theta}{z_c}^2+u_{3,\theta}{z_c}^3+w_{0,s}w_{0,\theta}\right]$$
$$+v_{0,s}+v_{1,s}z_c+v_{2,s}{z_c}^2+v_{3,s}{z_c}^3$$

It is assumed that core is perfectly bonded to the face sheets. So, the compatibility conditions between core and face-sheets which obtained by Lagrange multipliers in Eq. (9) are as follows:

$$u_o(z_o=h_o/2)=u_c(z_c=-h_c/2) \quad (29)$$

$$v_o(z_o=h_o/2)=v_c(z_c=-h_c/2) \quad (30)$$

$$w_o=w_c(z_c=-h_c/2) \quad (31)$$

$$u_c(z_c=h_c/2)=u_i(z_i=-h_i/2) \quad (32)$$

$$v_c(z_c=h_c/2)=v_i(z_i=-h_i/2) \quad (33)$$

$$w_c(z_c=h_c/2)=w_i \quad (34)$$

Based on compatibility conditions, the displacements of the face-sheets are dependent to the core, so the unknown decrease to fifteen and the number of the governing equations are fifteen.

$$+r\frac{h_o}{2}N_{ss,s}^{o}-rM_{ss,s}^{o}+\frac{h_o}{2}N_{s\theta,\theta}^{o}-M_{s\theta,\theta}^{o}+ \quad (35)$$
$$rN_{sz}^{o}-\frac{h_o}{2}n_s^{o}=0$$

$$+\frac{h_o}{2}N_{\theta\theta,\theta}^{o}-M_{\theta\theta,\theta}^{o}+\frac{h_o}{2}rN_{s\theta,s}^{o}-rM_{s\theta,s}^{o}- \quad (36)$$
$$M_{\theta z}^{o}+rN_{\theta z}^{o}+\frac{h_o}{2}N_{\theta z}^{o}-\frac{h_o}{2}n_s^{o}=0$$

$$-r\frac{h_i}{2}N_{ss,s}^{i}-rM_{ss,s}^{i}-\frac{h_i}{2}N_{s\theta,\theta}^{i}-M_{s\theta,\theta}^{i}+ \quad (37)$$
$$rN_{sz}^{i}+\frac{h_i}{2}n_s^{i}=0$$

$$-\frac{h_i}{2}N_{\theta\theta,\theta}^{i}-M_{\theta\theta,\theta}^{i}-\frac{h_i}{2}rN_{s\theta,s}^{i}-rM_{s\theta,s}^{i}-M_{\theta z}^{i}+ \quad (38)$$
$$rN_{\theta z}^{i}-\frac{h_i}{2}N_{\theta z}^{i}+\frac{h_i}{2}n_s^{i}=0$$

$$-rN_{ss,s}^{o}-N_{s\theta,\theta}^{o}-rN_{ss,s}^{i}-N_{s\theta,\theta}^{i}-rR_{ss,s}^{c} \quad (39)$$
$$-Q_{s\theta,\theta}^{c}+n_s^{o}+n_s^{i}=0$$

$$+r\frac{h_c}{2}N_{ss,s}^{o}-r\frac{h_c}{2}N_{ss,s}^{i}+\frac{h_c}{2}N_{s\theta,\theta}^{o}-\frac{h_c}{2}N_{s\theta,\theta}^{i}- \quad (40)$$
$$rM_{s1,s}^{i}-M_{Q1s\theta,\theta}^{c}+rQ_{sz}^{c}+\frac{h_c}{2}n_s^{o}+\frac{h_c}{2}n_s^{i}=0$$

$$-r\frac{h_c^2}{4}N_{ss,s}^{o}-r\frac{h_c^2}{4}N_{ss,s}^{i}-\frac{h_c^2}{4}N_{s\theta,\theta}^{o}-\frac{h_c^2}{4}N_{s\theta,\theta}^{i} \quad (41)$$
$$-rM_{s2,s}^{i}-M_{Q2s\theta,\theta}^{c}+2rM_{Q1sz}^{c}+\frac{h_c^2}{4}n_s^{o}+\frac{h_c^2}{4}n_s^{i}=0$$

$$+r\frac{h_c^3}{8}N_{ss,s}^{o}-r\frac{h_c^3}{8}N_{ss,s}^{i}+\frac{h_c^3}{8}N_{s\theta,\theta}^{o}-\frac{h_c^3}{8}N_{s\theta,\theta}^{i}- \quad (42)$$
$$rM_{s3,s}^{i}-M_{Q3s\theta,\theta}^{c}+3rM_{Q2sz}^{c}-\frac{h_c^3}{8}n_s^{o}+\frac{h_c^3}{8}n_s^{i}=0$$

$$-N_{\theta\theta,\theta}^{o}-N_{\theta\theta,\theta}^{i}-rN_{s\theta,s}^{o}-rN_{s\theta,s}^{i}-N_{\theta z}^{o}-N_{\theta z}^{i} \quad (43)$$
$$-R_{\theta,\theta}^{c}-rQ_{s\theta,s}^{c}-Q_{\theta z}^{c}+n_s^{o}+n_s^{i}=0$$

$$+\frac{h_c}{2}N^{o}_{\theta\theta,\theta}-\frac{h_c}{2}N^{i}_{\theta\theta,\theta}+r\frac{h_c}{2}N^{o}_{s\theta,s}-r\frac{h_c}{2}N^{i}_{s\theta,s}+$$
$$\frac{h_c}{2}N^{o}_{\theta z}-\frac{h_c}{2}N^{i}_{\theta z}-M^{c}_{\theta 1,\theta}-rM^{c}_{Q1s\theta,s}-M^{c}_{Q1\theta z} \quad (44)$$
$$+rQ^{c}_{\theta z}-\frac{h_c}{2}n^{o}_{s}+\frac{h_c}{2}n^{i}_{s}=0$$

$$-\frac{h_c^2}{4}N^{o}_{\theta\theta,\theta}-\frac{h_c^2}{4}N^{i}_{\theta\theta,\theta}-r\frac{h_c^2}{4}N^{o}_{s\theta,s}-r\frac{h_c^2}{4}N^{i}_{s\theta,s}-$$
$$\frac{h_c^2}{4}N^{o}_{\theta z}-\frac{h_c^2}{4}N^{i}_{\theta z}-M^{c}_{\theta 2,\theta}-rM^{c}_{Q2s\theta,s}-M^{c}_{Q2\theta z} \quad (45)$$
$$+2rM^{c}_{Q1\theta z}+\frac{h_c^2}{4}n^{o}_{s}+\frac{h_c^2}{4}n^{i}_{s}=0$$

$$+\frac{h_c^3}{8}N^{o}_{\theta\theta,\theta}-\frac{h_c^3}{8}N^{i}_{\theta\theta,\theta}+r\frac{h_c^3}{8}N^{o}_{s\theta,s}-r\frac{h_c^3}{8}N^{i}_{s\theta,s}$$
$$+\frac{h_c^3}{8}N^{o}_{\theta z}-\frac{h_c^3}{8}N^{i}_{\theta z}-M^{c}_{\theta 3,\theta}-rM^{c}_{Q3s\theta,s}-M^{c}_{Q3\theta z} \quad (46)$$
$$+3rM^{c}_{Q2\theta z}-\frac{h_c^3}{8}n^{o}_{s}+\frac{h_c^3}{8}n^{i}_{s}=0$$

$$-N^{o}(w^{c}_{0})-N^{i}(w^{c}_{0})-N^{c}(w^{c}_{0})+\frac{h_c}{2}N^{o}(w^{c}_{1})$$
$$-\frac{h_c}{2}N^{i}(w^{c}_{1})-\frac{h_c^2}{4}N^{o}(w^{c}_{2})-\frac{h_c^2}{4}N^{i}(w^{c}_{2})$$
$$-N^{oT}(w^{c}_{0})-N^{iT}(w^{c}_{0})-N^{cT}(w^{c}_{0})+\frac{h_c}{2}N^{oT}(w^{c}_{1}) \quad (47)$$
$$-\frac{h_c}{2}N^{iT}(w^{c}_{1})-\frac{h_c^2}{4}N^{oT}(w^{c}_{2})-\frac{h_c^2}{4}N^{iT}(w^{c}_{2})$$
$$+N^{o}_{\theta\theta}+N^{i}_{\theta\theta}-rN^{o}_{sz,s}-rN^{i}_{sz,s}-N^{o}_{\theta z,\theta}-N^{i}_{\theta z,\theta}$$
$$+-R^{c}_{\theta}-rQ^{c}_{sz,s}+n^{o}_{s}+n^{i}_{s}=0$$

$$+\frac{h_c}{2}N^{o}(w^{c}_{0})-\frac{h_c}{2}N^{i}(w^{c}_{0})-\frac{h_c^2}{4}N^{o}(w^{c}_{1})$$
$$-\frac{h_c^2}{4}N^{i}(w^{c}_{1})+\frac{h_c^3}{8}N^{o}(w^{c}_{2})-\frac{h_c^3}{8}N^{i}(w^{c}_{2})$$
$$+\frac{h_c}{2}N^{oT}(w^{c}_{0})-\frac{h_c}{2}N^{iT}(w^{c}_{0})-\frac{h_c^2}{4}N^{oT}(w^{c}_{1})$$
$$-\frac{h_c^2}{4}N^{iT}(w^{c}_{1})+\frac{h_c^3}{8}N^{oT}(w^{c}_{2})-\frac{h_c^3}{8}N^{iT}(w^{c}_{2}) \quad (48)$$
$$-\frac{h_c}{2}N^{o}_{\theta\theta}+\frac{h_c}{2}N^{i}_{\theta\theta}+\frac{h_c}{2}rN^{o}_{sz,s}-\frac{h_c}{2}rN^{i}_{sz,s}+\frac{h_c}{2}N^{o}_{\theta z,\theta}$$
$$-\frac{h_c}{2}N^{i}_{\theta z,\theta}+M^{c}_{\theta 1}+rR^{c}_{z}-rM^{c}_{Q1sz,s}-\frac{h_c}{2}n^{o}_{s}+\frac{h_c}{2}n^{i}_{s}=0$$

$$-\frac{h_c^2}{4}N^{o}(w^{c}_{0})-\frac{h_c^2}{4}N^{i}(w^{c}_{0})+\frac{h_c^3}{8}N^{o}(w^{c}_{1})-$$
$$\frac{h_c^3}{8}N^{i}(w^{c}_{1})-\frac{h_c^4}{16}N^{o}(w^{c}_{2})-\frac{h_c^4}{16}N^{i}(w^{c}_{2})$$
$$-\frac{h_c^2}{4}N^{oT}(w^{c}_{0})-\frac{h_c^2}{4}N^{iT}(w^{c}_{0})+\frac{h_c^3}{8}N^{oT}(w^{c}_{1})$$
$$-\frac{h_c^3}{8}N^{iT}(w^{c}_{1})-\frac{h_c^4}{16}N^{oT}(w^{c}_{2})-\frac{h_c^4}{16}N^{iT}(w^{c}_{2}) \quad (49)$$
$$+\frac{h_c^2}{4}N^{o}_{\theta\theta}-\frac{h_c^2}{4}N^{i}_{\theta\theta}-\frac{h_c^2}{4}rN^{o}_{sz,s}-\frac{h_c^2}{4}rN^{i}_{sz,s}-$$
$$\frac{h_c^2}{4}N^{o}_{\theta z,\theta}-\frac{h_c^2}{4}N^{i}_{\theta z,\theta}+M^{c}_{\theta 2}+2rM^{c}_{z1}-rM^{c}_{Q2sz,s}$$
$$+\frac{h_c^2}{4}n^{o}_{s}+\frac{h_c^2}{4}n^{i}_{s}=0$$

where $N^{j}(w^{c}_{l})$ is defined as follows (Kheirikhah, Khalili et al. 2012):

$$N^{j}(w^{c}_{l})=rN^{j}_{ss,s}w^{c}_{l,s}+rN^{j}_{ss}w^{c}_{l,ss}+N^{j}_{s\theta,s}w^{c}_{l,\theta} \quad (50)$$
$$+2N^{j}_{s\theta}w^{c}_{l,s\theta}+1/r\,N^{j}_{\theta\theta,\theta}w^{c}_{l,\theta}+1/r\,N^{j}_{\theta\theta}w^{c}_{l,\theta\theta}$$
$$;j=(o,i,c),l=(0,1,2)$$

"A", "B" and "D" are the constant coefficients of stretching, the bending-stretching, and bending stiffness:

$$\begin{Bmatrix}N^{j}_{ss}\\N^{j}_{\theta\theta}\\N^{j}_{s\theta}\end{Bmatrix}=\begin{bmatrix}A_{11}&A_{12}&0\\A_{12}&A_{22}&0\\0&0&A_{66}\end{bmatrix}\begin{Bmatrix}\varepsilon^{(0)}_{ssj}\\\varepsilon^{(0)}_{\theta\theta j}\\\varepsilon^{(0)}_{s\theta j}\end{Bmatrix}+$$
$$\begin{bmatrix}B_{11}&B_{12}&0\\B_{12}&B_{22}&0\\0&0&B_{66}\end{bmatrix}\begin{Bmatrix}\varepsilon^{(1)}_{ssj}\\\varepsilon^{(1)}_{\theta\theta j}\\\varepsilon^{(1)}_{s\theta j}\end{Bmatrix}-\begin{Bmatrix}N^{Tj}_{ss}\\N^{Tj}_{\theta\theta}\\0\end{Bmatrix} \quad (51)$$

$$\begin{Bmatrix}M^{j}_{ss}\\M^{j}_{\theta\theta}\\M^{j}_{s\theta}\end{Bmatrix}=\begin{bmatrix}B_{11}&B_{12}&0\\B_{12}&B_{22}&0\\0&0&B_{66}\end{bmatrix}\begin{Bmatrix}\varepsilon^{(0)}_{ssj}\\\varepsilon^{(0)}_{\theta\theta j}\\\varepsilon^{(0)}_{s\theta j}\end{Bmatrix}+$$
$$\begin{bmatrix}D_{11}&D_{12}&0\\D_{12}&D_{22}&0\\0&0&D_{66}\end{bmatrix}\begin{Bmatrix}\varepsilon^{(1)}_{ssj}\\\varepsilon^{(1)}_{\theta\theta j}\\\varepsilon^{(1)}_{s\theta j}\end{Bmatrix}-\begin{Bmatrix}M^{Tj}_{ss}\\M^{Tj}_{\theta\theta}\\0\end{Bmatrix} \quad (52)$$

$$\begin{Bmatrix}N^{j}_{sz}\\N^{j}_{\theta z}\end{Bmatrix}=\frac{\pi^2}{12}\begin{bmatrix}A_{44}&0\\0&A_{55}\end{bmatrix}\begin{Bmatrix}\gamma^{(0)}_{szj}\\\gamma^{(0)}_{\theta zj}\end{Bmatrix}+$$
$$\frac{\pi^2}{12}\begin{bmatrix}B_{44}&0\\0&B_{55}\end{bmatrix}\begin{Bmatrix}\gamma^{(1)}_{szj}\\\gamma^{(1)}_{\theta zj}\end{Bmatrix},\qquad j=(o,i) \quad (53)$$

$$M^{j}_{\theta z}=\frac{\pi^2}{12}B_{55}\gamma^{(0)}_{\theta zj}+\frac{\pi^2}{12}D_{55}\gamma^{(1)}_{\theta zj}$$

Also the strain components in the Eqs. (51-53) are defined

as:

$$\begin{Bmatrix} \varepsilon_{ssj}^{(0)} \\ \varepsilon_{\theta\theta j}^{(0)} \\ \varepsilon_{s\theta j}^{(0)} \end{Bmatrix} = \begin{Bmatrix} u_{0j,s} \\ \frac{1}{r}\left(v_{0j,\theta} + w_j\right) \\ \frac{1}{r}u_{0j,\theta} + v_{0j,s} \end{Bmatrix} \quad , \tag{54}$$

$$\begin{Bmatrix} \varepsilon_{ssj}^{(1)} \\ \varepsilon_{\theta\theta j}^{(1)} \\ \varepsilon_{s\theta j}^{(1)} \end{Bmatrix} = \begin{Bmatrix} \phi_{s,s}^{j} \\ \frac{1}{r}\phi_{\theta,\theta}^{j} \\ \frac{1}{r}\phi_{s,\theta}^{j} + \phi_{\theta,s}^{j} \end{Bmatrix}$$

$$\begin{Bmatrix} \gamma_{szj}^{(0)} \\ \gamma_{\theta zj}^{(0)} \end{Bmatrix} = \begin{Bmatrix} w_{j,s} + \phi_s^j \\ \frac{1}{r}\left(w_{j,\theta} - v_{0j}\right) + \phi_\theta^j \end{Bmatrix} \quad , \tag{55}$$

$$\begin{Bmatrix} \gamma_{szj}^{(1)} \\ \gamma_{\theta zj}^{(1)} \end{Bmatrix} = \begin{Bmatrix} 0 \\ \frac{-\phi_\theta^j}{r} \end{Bmatrix}$$

It should be noted that $\frac{\pi^2}{12}$ is the shear correction factor in FSDT. Also, $N_{ss}^{Tj}, N_{\theta\theta}^{Tj}, M_{ss}^{Tj}$ and $M_{\theta\theta}^{Tj}$ are the thermal stress resultants. "A" is the stretching stiffness; "B" is the bending-stretching stiffness; and "D" is the bending stiffness; which are constant coefficients and express as:

$$N_{ss}^{Tj} = N_{\theta\theta}^{Tj} = \int_{-\frac{h_j}{2}}^{\frac{h_j}{2}} \frac{E_j(z_j,T_j)}{1-\upsilon_j(z_j,T_j)}.\alpha_j(z_j,T_j).\Delta T_j\, dz_j \tag{56}$$

$$, \quad j = (o,i)$$

$$M_{ss}^{Tj} = M_{\theta\theta}^{Tj} = \int_{-\frac{h_j}{2}}^{\frac{h_j}{2}} \frac{z_j.E_j(z_j,T_j)}{1-\upsilon_j(z_j,T_j)}.\alpha_j(z_j,T_j).\Delta T_j\, dz_j \tag{57}$$

$$, \quad j = (o,i)$$

$$\begin{Bmatrix} A_{11}^{j} \\ B_{11}^{j} \\ D_{11}^{j} \end{Bmatrix} = \begin{Bmatrix} A_{22}^{j} \\ B_{22}^{j} \\ D_{22}^{j} \end{Bmatrix} = \int_{-\frac{h_j}{2}}^{\frac{h_j}{2}} \left[\frac{E_j\left(z_j,T_j\right)}{1-\left(\upsilon_j\left(z_j,T_j\right)\right)^2}\right] \begin{Bmatrix} 1 \\ z_j \\ z_j^{\,2} \end{Bmatrix} dz_j \tag{58}$$

$$\begin{Bmatrix} A_{12}^{j} \\ B_{12}^{j} \\ D_{12}^{j} \end{Bmatrix} = \int_{-\frac{h_j}{2}}^{\frac{h_j}{2}} \left[\frac{\upsilon_j\left(z_j,T_j\right)\times E_j\left(z_j,T_j\right)}{1-\left(\upsilon_j\left(z_j,T_j\right)\right)^2}\right] \begin{Bmatrix} 1 \\ z_j \\ z_j^{\,2} \end{Bmatrix} dz_j \tag{59}$$

$$\begin{Bmatrix} A_{66}^{j} \\ B_{66}^{j} \\ D_{66}^{j} \end{Bmatrix} = \int_{-\frac{h_j}{2}}^{\frac{h_j}{2}} \left[\frac{E_j\left(z_j,T_j\right)}{2\left(1+\upsilon_j\left(z_j,T_j\right)\right)}\right] \begin{Bmatrix} 1 \\ z_j \\ z_j^{\,2} \end{Bmatrix} dz_j \tag{60}$$

On where $E_j(z_j,T_j)$, $\upsilon_j(z_j,T_j)$ and $\alpha_j(z_j,T_j)$, $j = (o,i)$ are the modulus of elasticity, Poisson's ratio and the thermal expansion coefficient of the FG face sheets, respectively, and introduced by power-law function of FGMs. "o" and "i" refer to the outer and inner face sheet layers, respectively. And also, twenty three stress resultants of the core are defined as:

$$\left\{Q_{sz}^{c}, M_{Q1sz}^{c}, M_{Q2sz}^{c}, M_{Q3sz}^{c}\right\} = \int_{-\frac{h_c}{2}}^{\frac{h_c}{2}} \left(1, z_c, z_c^{\,2}, z_c^{\,3}\right)\tau_{sz}^{c}\, dz_c \tag{61}$$

$$\left\{Q_{\theta z}^{c}, M_{Q1\theta z}^{c}, M_{Q2\theta z}^{c}, M_{Q3\theta z}^{c}\right\} = \int_{-\frac{h_c}{2}}^{\frac{h_c}{2}} \left(1, z_c, z_c^{\,2}, z_c^{\,3}\right)\tau_{\theta z}^{c}\, dz_c \tag{62}$$

$$\left\{R_{z}^{c}, M_{z1}^{c}, M_{z2}^{c}\right\} = \int_{-\frac{h_c}{2}}^{\frac{h_c}{2}} \left(1, z_c, z_c^{\,2}\right)\sigma_{zz}^{c}\, dz_c \tag{63}$$

$$\left\{Q_{s\theta}^{c}, M_{Q1s\theta}^{c}, M_{Q2s\theta}^{c}, M_{Q3s\theta}^{c}\right\} = \int_{-\frac{h_c}{2}}^{\frac{h_c}{2}} \left(1, z_c, z_c^{\,2}, z_c^{\,3}\right)\tau_{s\theta}^{c} dz_c \tag{64}$$

$$\left\{R_{s}^{c}, M_{s1}^{c}, M_{s2}^{c}, M_{s3}^{c}\right\} = \int_{-\frac{h_c}{2}}^{\frac{h_c}{2}} \left(1, z_c, z_c^{\,2}, z_c^{\,3}\right)\sigma_{ss}^{c} dz_c \tag{65}$$

$$\left\{R_{\theta}^{c}, M_{\theta1}^{c}, M_{\theta2}^{c}, M_{\theta3}^{c}\right\} = \int_{-\frac{h_c}{2}}^{\frac{h_c}{2}} \left(1, z_c, z_c^{\,2}, z_c^{\,3}\right)\sigma_{\theta\theta}^{c} dz_c \tag{66}$$

where Finally, by substituting the high order stress resultants in terms of the kinematic relations, the equations are derived in terms of the nine unknowns.

Eq. (50) can be rewritten as (Kheirikhah, Khalili et al. 2012):

$$N(w_l^{c}) = r\hat{N}_{ss,s}^{j} w_{l,s}^{c} + r\hat{N}_{ss}^{j} w_{l,ss}^{c} + \hat{N}_{s\theta,s}^{j} w_{l,\theta}^{c} + 2\hat{N}_{s\theta}^{j} w_{l,s\theta}^{c} + \tfrac{1}{r}\hat{N}_{\theta\theta,\theta}^{j} w_{l,\theta}^{c} + \tfrac{1}{r}\hat{N}_{\theta\theta}^{j} w_{l,\theta\theta}^{c} \tag{67}$$

$; j = (o,i,c), l = (0,1,2)$

where $\hat{N}_{ss}^{j}, \hat{N}_{\theta\theta}^{j}$ *and* $\hat{N}_{s\theta}^{j}$ are the external in-plane loads exerted to the top and bottom face sheets and the core. Therefore

$$N(w_l^{c}) = \hat{N}_{ss}^{j} w_{l,ss}^{c} + 2\hat{N}_{s\theta}^{j} w_{l,s\theta}^{c} + \hat{N}_{\theta\theta}^{j} w_{l,\theta\theta}^{c} \tag{68}$$

The axial in-plane compressive loads, $\hat{N}_{ss}^{j}$, are the parts of total external load, $\hat{N}_0$, as follows:

$$N_{ss}^{o} + N_{ss}^{i} + N_{ss}^{c} = -N_0 \tag{69}$$

Hence, in this analysis, uniform state of strain for the face sheets and the core is assumed. At edges "s=0" or "s=L" and with a little simplification the equilibrium equations can be defined as:

$$\frac{N_{ss}^{o}}{h_o \bar{E}_o} = \frac{N_{ss}^{i}}{h_i \bar{E}_i} = \frac{N_{ss}^{c}}{h_c \bar{E}_c} \tag{70}$$

where $\bar{E}_j$ is the equilibrium elasticity modulus of the layers that are defined as:

$$\bar{E}_j = \frac{\int_{-h_j/2}^{h_j/2} E_j(z_j) dz_j}{h_j}; j = (o,i,c) \tag{71}$$

Hence, by using of Eq. (70) and (71), the external in-plane loads exerted to the face sheets and the core along the "s" direction can be obtained as:

$$\begin{Bmatrix} N_{ss}^{o} \\ N_{ss}^{i} \\ N_{ss}^{c} \end{Bmatrix} = \frac{-N_0}{h_o \bar{E}_o + h_i \bar{E}_i + h_c \bar{E}_c} \begin{Bmatrix} h_o \bar{E}_o \\ h_i \bar{E}_i \\ h_c \bar{E}_c \end{Bmatrix} \tag{72}$$

3. Galerkin method

A Galerkin procedure is applied to solve the governing equations of two types of FG sandwich cylindrical shells, with trigonometric shape functions, which satisfy the boundary conditions. The shape functions of simply supported boundary condition are expressed as follows:

$$u_{0k} = C_{uk} cos\left(\frac{m\pi s}{L}\right)\cos(n\theta);\ k = (o,i,c) \tag{73}$$

$$v_{0k} = C_{vk} sin\left(\frac{m\pi s}{L}\right)\sin(n\theta) \tag{74}$$

$$w_{0k} = C_{wk} sin\left(\frac{m\pi s}{L}\right)\cos(n\theta) \tag{75}$$

$$\phi_s^{j} = C_{\phi sj} cos\left(\frac{m\pi s}{L}\right)\cos(n\theta);\ j = (o,i) \tag{76}$$

$$\phi_\theta^{j} = C_{\phi\theta j} cos\left(\frac{m\pi s}{L}\right)\cos(n\theta) \tag{77}$$

And the shape functions of the clamped boundary condition can be expressed as(Rahmani and Mohammadi 2021)*:*

$$u_{ck} = C_{uk} \sin\left(\frac{m\pi}{L}s\right)\cos(n\theta), k = (0,1,2,3) \tag{78}$$

$$v_{ck} = C_{vk} sin\left(\frac{m\pi s}{L}\right)\sin(n\theta) \tag{79}$$

$$w_{ck} = C_{wk}\left(\sinh(\frac{\lambda_m s}{L}) - \sin(\frac{\lambda_m s}{L}) + \gamma_m(\cos h(\frac{\lambda_m s}{L}) - \cos(\frac{\lambda_m s}{L}))\right)\cos(n\theta) \tag{80}$$

$$\phi_s^{j} = C_{\phi sj} cos\left(\frac{m\pi s}{L}\right)\cos(n\theta), j = (o,i) \tag{81}$$

$$\phi_\theta^{j} = C_{\phi\theta j} sin\left(\frac{m\pi s}{L}\right)\sin(n\theta) \tag{82}$$

which γ_m and λ_m should satisfy the conditions as follow:

$$\cos\lambda_m . \cosh\lambda_m = 1 \tag{83}$$

$$\gamma_m = \frac{\sinh\lambda_m - \sin\lambda_m}{\cos\lambda_m - \cosh\lambda_m} \quad m = (1,2,3,...) \tag{84}$$

Nine where "$a_m = m\pi / L$", "m" is the wave number and "$C_{uk}, C_{wk}, C_{\phi j}$"are the nine unknown constants of the shape functions. These fifteen equations can be displayed with a 15×15 matrix as follows:

$$(k_m - N_0 \times G_m)C_m = 0 \tag{85}$$

4. Verification and numerical method

To verify the approach of this study, present results are compared with the results of the literatures (Fard and Livani 2015), (Vodenitcharova and Ansourian 1996), (Shen 2003) and (Khazaeinejad and Najafizadeh 2010). Consider a simply supported metallic isotropic cylindrical shell with structural parameters such as h = 0.001m, L=2R, E=200 GPa and ν=0.3. These comparisons are shown in Table 1.

Table 1
Buckling pressure for cylindrical isotropic panel

L/R	Present study	(Fard and Livani 2015)	(Vodenitcharova and Ansourian 1996)	(Shen 2003)	(Khazaeinejad and Najafizadeh 2010)
0.5	2765.4	2768.1	2766.2	2761.4	2767.4
1	1272.9	1272.0	1269.6	1272.6	1273.1
2	611.7	611.6	607.3	611.7	611.7
3	408.5	411.9	407.2	402.6	412.6

Because, theory and solution method of the present analysis are different with reference [30], a discrepancy is found in the results. Now, another numerical problem will be discussed to more investigation the present approach. Consider two kinds of FG sandwich cylindrical shell. In type-I, the face sheets interior planes and the core are made of the zirconium dioxide and the outer planes of the faces are made of silicon nitride. In type-II, the interior plane of the core and inner face sheet are made of the zirconium dioxide and the outer plane of the core and outer face sheet are made of silicon nitride. The temperature-dependent properties of constituent materials which is introduced by Eq. (1) are available in reference (Reddy 2003). In general, "ht-hc-hb" sandwich shell is a structure with the indices of top face sheet thickness, core thickness and bottom face sheet thickness equal to "ht", "hc" and "hb", respectively. Therefore, in 1-8-1 sandwich, the thickness of the core is eight times of each face sheet thickness. For simplicity, the non-dimensional critical load parameter is defined as follows:

$$N_{cr} = \frac{N_0}{10^9} \tag{86}$$

The material properties of structures are affected in high temperature conditions. Based on Eq. (1), increasing the temperature reduces the Young modulus and density of metal and ceramic. As a result, the strength of the panels reduces, which is an important reason in decreasing the critical load in high temperature conditions. Figure 2 shows the critical parameter variation versus the temperature for two types of 1-8-1 FG sandwich cylindrical shell with simply supported (S-S) and clamped (C-C) boundary conditions. Geometrical parameters are "h=0.02m, R/h=50, L=2R". By increasing the temperature, the critical load parameters decrease. As shown in Figure 2, when N=0, the FG layers are made of full ceramic, as a result, the stability and resistant against the high temperature conditions are more than the other values of "N", so critical load parameters are higher than others. By increasing the power law index, "N", the amount of the ceramic reduces in the structure which causes the young modulus of the FGM and the stability of the structures decrease. In 1-8-1 sandwich, the core thickness is eight times of the face sheet, so in sandwich type-II which has a FG core, the amount of the ceramic is more than the type-I. As a result, the stability and resistant of the type-II is higher than the type-I, so the critical load parameter of the type-II is higher. When N=2, in sandwiches type-I and type-II with simply supported boundary condition (S-S), the amount of the ceramic is low in the FG layers, so, in the high temperature the stability of the structure is low. The critical load parameters of simply supported boundary conditions in both types, are lower than the clamped (C-C) boundary conditions. Based on the Fig. 2, the sandwich type-II with the clamped boundary condition is most resistant sandwich in the high temperature environments. Also, in sandwich type-I (S-S), when "N=0", by increasing the temperature, the critical load parameter decreases 39.94%, for "N=1" and "N=2" it decreases 45.15%, and 46.90%, respectively. In sandwich type-I (C-C), when "N=0", by increasing the temperature, the critical load parameter decreases 46.59.%, for "N=1" and "N=2" it decreases 50.92%, and 52.11%, respectively. And in sandwich type-II (S-S), when "N=0", by increasing the temperature, the critical load parameter decreases 17.14%, for "N=1" and "N=2" it decreases 28.97%, and 33.71%, respectively. And in sandwich type-II (C-C), when "N=0", by increasing the temperature, the critical load parameter decreases 11.63%, for "N=1" and "N=2" it decreases 24.90%, and 29.88%, respectively. As shown in the results, the sandwich type-II is proper than the type-I in the same boundary condition for using in the thermal conditions.

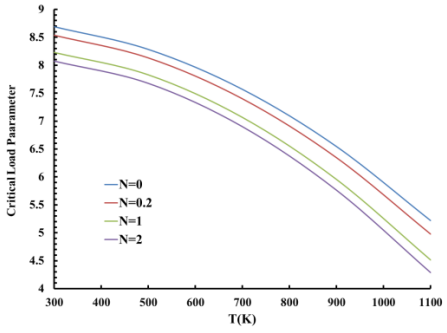

a. sandwich Type-I (S-S)

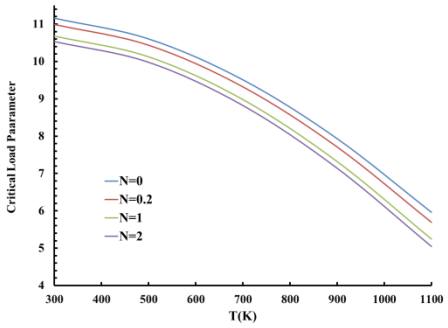

b. sandwich Type-I (C-C)

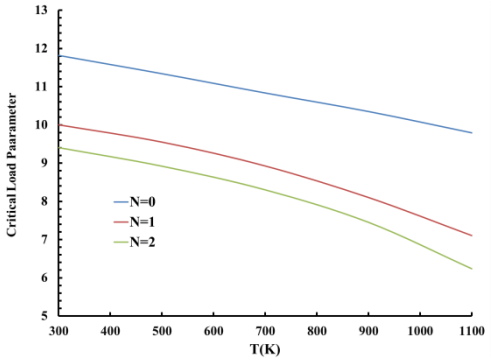

a. sandwich Type-II (S-S)

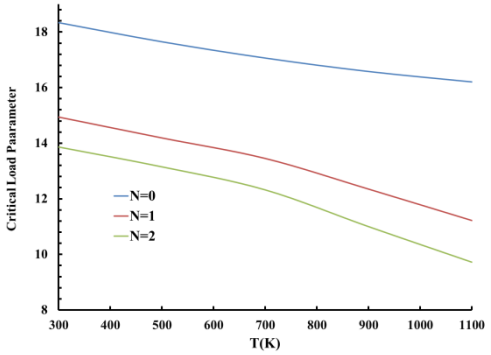

b. sandwich Type-II (C-C)

Fig .2. Critical load variation versus temperature in different types of sandwich cylindrical shell.

Figure 3 shows the effect of radius to thickness ratio (R/h) on the critical load parameter for 1-8-1 FG sandwich cylindrrrical shell in the simply supported (S-S) and clamped (C-C) boundary conditions. Geometrical parameters are “h = 0.02m, T=300K, L=2R, m=1”. By increasing the R/h ratio in a constant “N”, the critical load parameter shows different behaviors in the sandwiches. In the (S-S) cases of both types of sandwiches, incresing the ratio has a negligable effect on the critical load, but in the (C-C) cases, first the critical load reduses and after a certain value of R/h, the critical load incrreases. This shows that the boundary condition has an impressive effect on the stability of the structure. In both type of sandwiches, the critical load parameter of (S-S) boundary conditions, are too lower than (C-C) ones. It has been shown that in a same boundary condition, the critical load parameters of sandwich type-I are lower than sandwich type-II. Since the thicknesses of the FG layers in sandwich type-II are higher than the sandwich type-I, increasing the power law index, N, has more effect on type-II. Also, it is obvious that, by increasing the power law index, “N”, the critical load parameters decrease. For example, in sandwich type-I (S-S), for "R/h=50", by increasing “N”, the critical load parameter decreases 7.08%, and for “N=0”, by increasing this ratio, the critical load parameter decreases 0.14%. In sandwich type-I (C-C), for "R/h=50", by increasing “N”, the critical load parameter decreases 5.60%, and for “N=0”, by increasing this ratio, first the critical load parameter decreases 60.30%, then increases 18.06%. In sandwich type-II (S-S), for "R/h=50", by increasing “N”, the critical load parameter decreases 20.41%, and for “N=0”, by increasing this ratio, the critical load decreases 0.168%. And, in sandwich type-II (C-C), for "R/h=50", by increasing “N”, the critical load parameter decreases 24.39%, and for “N=0”, by increasing this ratio, first the critical load decreases 52.13%, then it increases 12.82%.

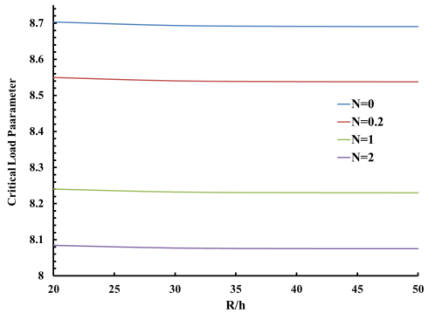

a. sandwich Type-I (S-S)

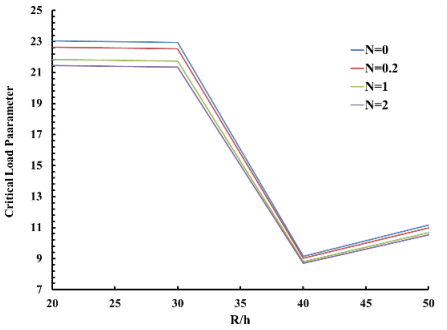

b. sandwich Type-I (C-C)

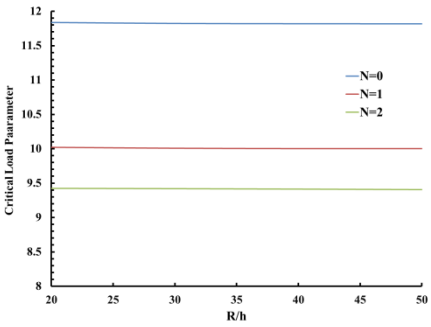

a. sandwich Type-II (S-S)

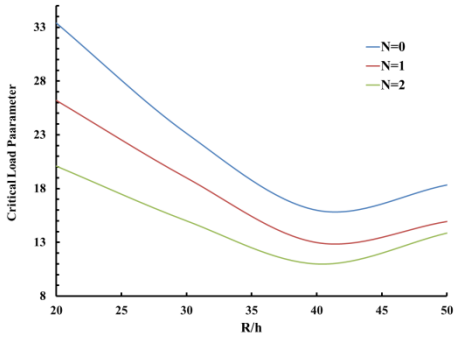

b. sandwich Type-II (C-C)

Fig .3. Critical load variation versus R/h ratio in different types of sandwich cylindrical shell.

Figure 4 shows the variation of the core to face sheet thickness ratio, “hc/ho”, on the critical load parameter in various power law indices and in a constant total thickness. Geometrical parameters are “h=0.02m, T=300K, m=1, R/h=50, L=2R”. When “hc/ho=0.5”, it means the face sheets thicknesses are two times of the core thickness, so it shows the results of the 2-1-2 sandwich. And, when “hc/ht=8”, it shows results of the 1-8-1 sandwich. In the case of (S-S) of sandwich type-I, by increasing the ratio, the critical load decreases, and in the case of (C-C) of sandwich type-I, by increasing the ratio, it increases. In the case of (S-S) of type-II, by increasing the ratio, first the critical load increases, but in the higher value of N, the behavior of critical load changes and it decreases. In the case of (C-C) of sandwich type-II, the critical load increases for all value of N. In the (S-S) of sandwich type-I, and in 2-1-2 sandwich, by increasing the ratio, the amount of ceramic decreases and the structure becomes softer, so the critical load parameters decrease. Since in 1-8-1 sandwich, the amount of ceramic is lower than 2-1-2 one, it is clear that the critical load parameter is lower. But the results in (C-C) of sandwich type-I are different and the 1-8-1 sandwich has taken more critical load. In the 1-8-1 sandwich type-II, the amount of ceramic is the most. By increasing the ratio in a constant thickness, the amount of ceramic increases and the structure becomes stiffer, so the critical load parameters increase at lower gradient indices, especially in “N=0”. Since in 1-8-1 sandwich type-II, the amount of ceramic is more than 2-1-2 one, it is clear that the critical load parameter is higher. But in the case of (S-S) of sandwich type-II, from a certain value of the power law index, by increasing ratio, the critical load of the 2-1-2 becomes more than 1-8-1 sandwiches. By increasing the power law index in a constant thickness, ceramic quantity of FG layer decreases, so, for all values of “hc/ho”, the critical load parameters decrease for both types of sandwiches. For sandwich type-I (S-S), in “hc/ho=0.5”, the critical load parameter decreases 20.46% when “N” is increased, and in “hc/ho=8”, the critical load parameter decrease 7.08. Also, for “N=0”, by increasing this ratio, the critical load decreases 28.22%, but for "N=2", it decreases 16.14%. For sandwich type-I (C-C), in “hc/ho=0.5”, the critical load parameter decreases 24.76% when “N” is increased, and in “hc/ho=8”, the critical load parameter decrease 5.60%. Also, for “N=0”, by increasing this ratio, the critical load increases 9.84%, but for "N=2", it incrreases 28.14%. For sandwich type-II (S-S), in “hc/ho=0.5”, the critical load parameter decrease 5.41% when “N” is increased, and in “hc/ho=8”, the critical load parameter decrease 20.41%. Also, for “N=0”, by increasing this ratio, the critical load increases 5.74%, but for "N=2", it decreases 10.72%. For sandwich type-II (C-C), in “hc/ho=0.5”, the critical load parameter decreases 7.95% when “N” is increased, and in “hc/ho=8”, the critical load parameter decreases 24.39%. Also, for “N=0”, by increasing this ratio, the critical load increases 23.37%, and for "N=2", it increase 6.71%.

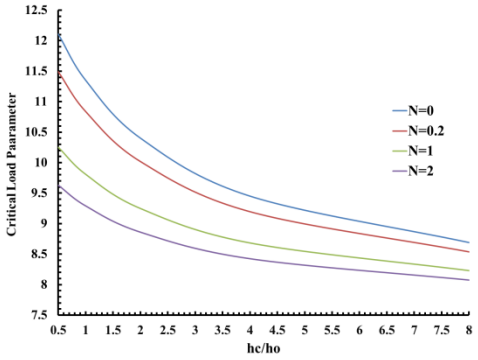

a. sandwich Type-I (S-S)

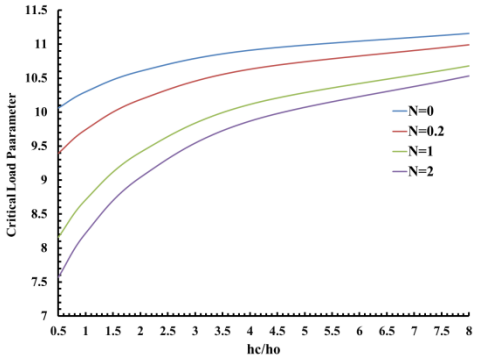

b. sandwich Type-I (C-C)

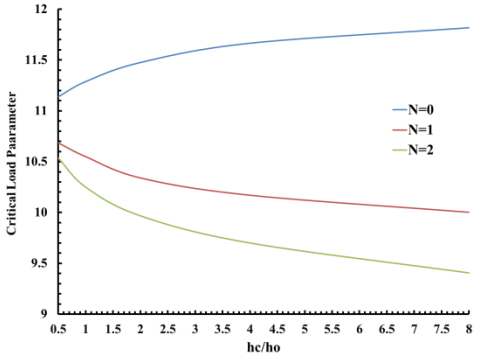

a. sandwich Type-II (S-S)

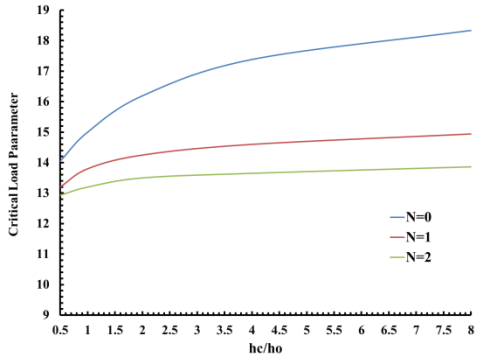

b. sandwich Type-II (C-C)

Fig .4. Critical load variation versus "hc/ho" ratio in different types of sandwich cylindrical shell.

Effect of the variation of the length to radius "L/R", on the critical load parameter in various power law indices for different simply supported and clamped FG sandwich cylindrical shell is depicted in Figure 5. Geometrical parameters are "T=300K, m=1, R/h=50, h=0.02m". In the (S-S) cases of both types of sandwich, by increasing the ratio, the critical load parameter increases. In the (C-C) case of both types of sandwich, the critical load parameter shows a oscillating behavior. The slope of increasing the critical load in the value of lower than 2 is sever for (S-S) sandwiches. For example, in (S-S) type-I, by increasing the ratio for N=0, the critical load increases 88.29% and in (S-S) type-II, it increases 88.44%.

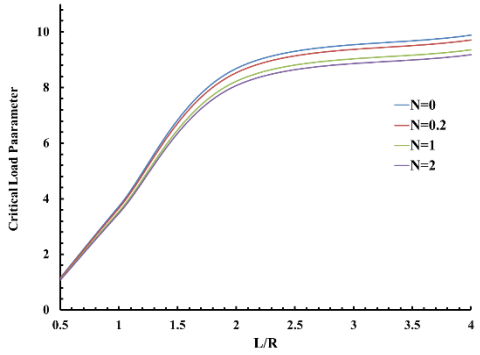

a. sandwich Type-I (S-S)

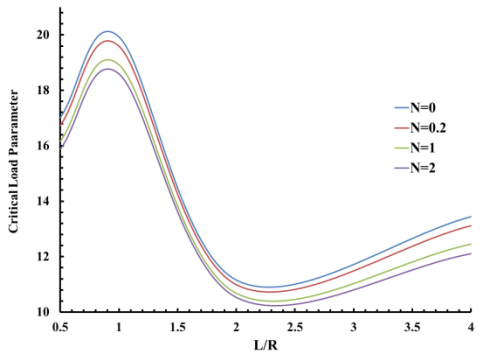

b. sandwich Type-I (C-C)

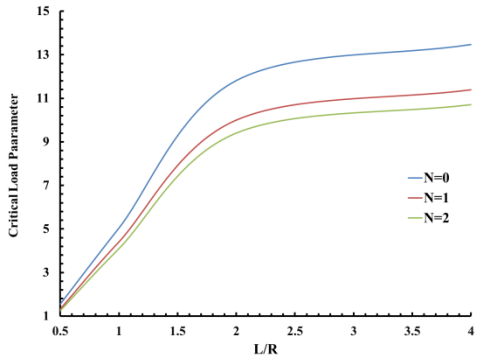

a. sandwich Type-II (S-S)

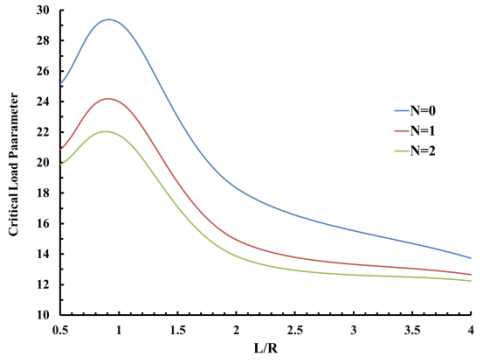

b. sandwich Type-II (C-C)

Fig .5. Critical load variation versus L/R ratio in different types of sandwich cylindrical shell.

In order to clearly understand the porosity influence, Fig. 6 and Fig. 7 show the effect of even and uneven porosity distributions on the critical load parameters of the different types of sandwich cylindrical shell, respectively. As shown in these figures, in both types of sandwiches, by increasing the porosity volume fraction, the critical load parameter decreases. These decreasing are stronger in the case of even porosity distribution in both sandwiches. In even distributions, porosities occur all over the cross-section of FG layer. While, in uneven distribution, porosities are available at middle zone of cross section. In sandwich type-I (S-S), and for the even case and "N=0", by increasing the volume fraction of the porosity, the critical load decreases 12.51%, and in the uneven case in "N=0", by increasing the volume fraction of the porosity, the critical load decreases 6.24%. In sandwich type-I (C-C), and for the even case and "N=0", by increasing the volume fraction of the porosity, the critical load decreases 3.73%, and in the uneven case in "N=0", by increasing the volume fraction of the porosity, the critical load decreases 1.52%. In sandwich type-II (S-S), and for the even case and "N=0", by increasing the volume fraction of the porosity, the critical load decreases 30.81%, and in the uneven case in "N=0", by increasing the volume fraction of the porosity, the critical load decreases 15.12%. And, in sandwich type-II (C-C), and for the even case and "N=0", by increasing the volume fraction of the porosity, the critical load decreases 25.08%, and in the uneven case in "N=0", by increasing the volume fraction of the porosity, the critical load

decreases 11.61%.

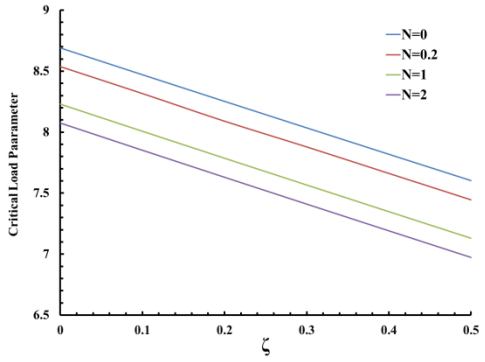

a. sandwich Type-I (S-S)

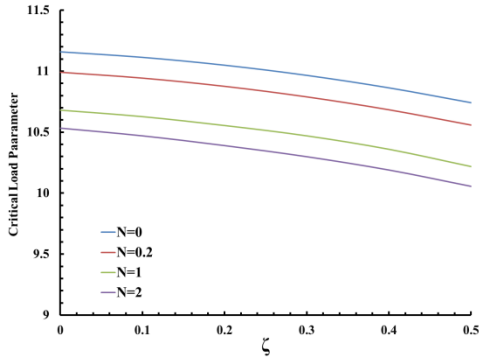

b. sandwich Type-I (C-C)

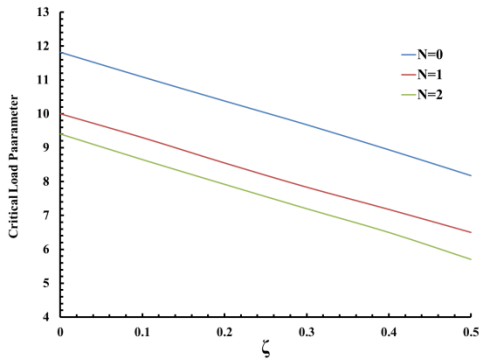

a. sandwich Type-II (S-S)

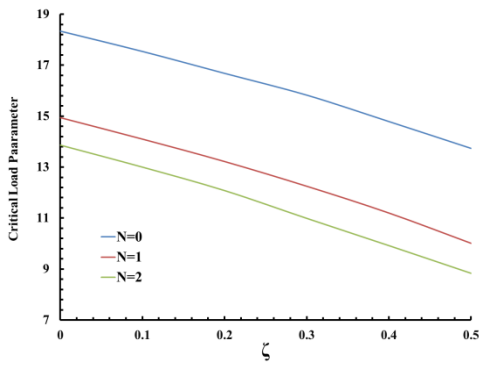

b. sandwich Type-II (C-C)

Fig .6. Critical load variation versus even porosity in different types of sandwich cylindrical shell.

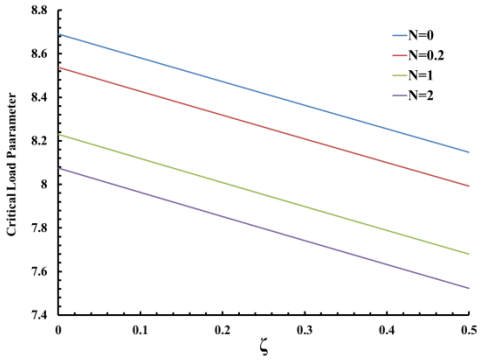

a. sandwich Type-I (S-S)

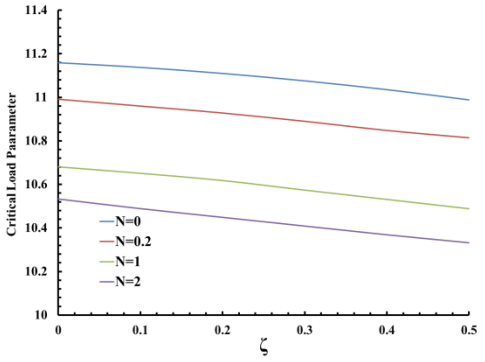

b. sandwich Type-I (C-C)

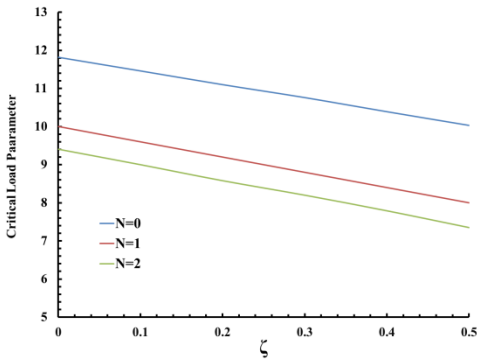

a. sandwich Type-II (S-S)

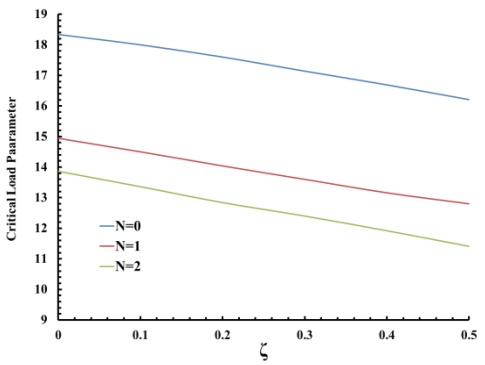

b. sandwich Type-II (C-C)

Fig .7. Critical load variation versus L/R ratio in different types of sandwich cylindrical shell.

5. Conclusion

By applying a modified high-order sandwich shell theory and considering the high-order stress resultants and thermal stress resultants, in plane stresses and thermal stresses, and nonlinear strains in face-sheets and core, buckling behavior of two types of porous FG sandwich cylindrical shell which were temperature dependent was investigated in this paper. The displacement fields of the face-sheets and the core were considered based on the first order shear deformation theory and the polynomial distributions, respectively. A power law distribution which modified by considering even and uneven porosity distributions was used to model the material properties of the FG layers. The FG layers were location dependent too. The governing equations were obtained by minimum potential energy principal and solved by using Galerkin method for simply supported and clamped boundary condition. Also, a method was applied to reduce the number of the equations. Effects of temperature, thickness, radius, and porosities distributions on the critical load were discussed. The following conclusion can be drawn:

- By increasing the temperature, the critical load parameters decrease.
- By increasing the power law index, the critical load parameters decrease.
- The stability of sandwich types-II is higher than type-I in the high temperature conditions.
- The critical load parameters of the sandwiches with simply supported boundary conditions are lower than sandwiches with clamped (C-C) boundary conditions.
- The sandwich type-II with the clamped boundary condition is most resistant sandwich in the high temperature environments.
- Increasing the radius to thickness ratio has a very small effect on the critical load of (S-S) sandwiches, but in (C-C) sndwiches first it reduses and after aa certain value increases. It shows the effect of boundary conditions on the behavior of the structure.
- Variation of the core to face-sheet thickness ratio has different effects on sandwiches.
- By increasing the L/R ratio, the critical load parameters increases in (S-S) sandwiches and shows a oscillating beahvior in (C-C) sandwiches.
- By increasing the porosity volume fraction in both even and uneven distributions, the critical load parameters decrease. Also, variation of critical load in even porosity case is more than uneven case.

References

Asadi, H., et al. (2015). "Enhanced thermal stability of functionally graded sandwich cylindrical shells by shape memory alloys." Smart Materials and Structures 24(4): 045022.

Balbin, I. U. and C. Bisagni (2021). "Buckling of sandwich cylindrical shells with shear deformable core through nondimensional parameters." Thin-Walled Structures 161: 107393.

Chan, D. Q., et al. (2021). "Nonlinear buckling and post-buckling of imperfect FG porous sandwich cylindrical panels subjected to axial loading under various boundary conditions." Acta Mechanica 232(3): 1163-1179.

Eslami, M. R., et al. (2018). Buckling and postbuckling of beams, plates, and shells, Springer.

Evkin, A. Y. (2019). Local buckling of cylindrical shells. Pogorelov's geometrical method. Problems of Nonlinear Mechanics and Physics of Materials, Springer: 369-391.

Fallah, F. and E. Taati (2019). "On the nonlinear bending and post-buckling behavior of laminated sandwich cylindrical shells with FG or isogrid lattice cores." Acta Mechanica 230(6): 2145-2169.

Fan, H. (2019). "Critical buckling load prediction of axially compressed cylindrical shell based on non-destructive probing method." Thin-Walled Structures 139: 91-104.

Fard, K. M. and M. Livani (2015). "The buckling of truncated conical sandwich panels under axial compression and external pressure." Proceedings of the Institution of Mechanical Engineers, Part C: Journal of Mechanical Engineering Science 229(11): 1965-1978.

Frostig, Y., et al. (1992). "High-order theory for sandwich-beam behavior with transversely flexible core." Journal of Engineering Mechanics 118(5): 1026-1043.

Gao, K., et al. (2018). "Nonlinear dynamic stability of the orthotropic functionally graded cylindrical shell surrounded by Winkler-Pasternak elastic foundation subjected to a linearly increasing load." Journal of Sound and Vibration 415: 147-168.

Ghahfarokhi, D. S. and G. Rahimi (2018). "An analytical approach for global buckling of composite sandwich cylindrical shells with lattice cores." International Journal of Solids and Structures 146: 69-79.

Han, Q., et al. (2017). "Thermal buckling analysis of cylindrical shell with functionally graded material coating." Composite Structures 181: 171-182.

Hieu, P. T. and H. V. Tung (2021). "Nonlinear buckling behavior of functionally graded material sandwich cylindrical shells with tangentially restrained edges subjected to external pressure and thermal loadings." Journal of Sandwich Structures & Materials 23(6): 2000-2027.

Khazaeinejad, P. and M. Najafizadeh (2010). "Mechanical buckling of cylindrical shells with varying material properties." Proceedings of the Institution of Mechanical Engineers, Part C: Journal of Mechanical Engineering Science 224(8): 1551-1557.

Kheirikhah, M., et al. (2012). "Biaxial buckling analysis of soft-core composite sandwich plates using improved high-order theory." European Journal of Mechanics-A/Solids 31(1): 54-66.

Lopatin, A. and E. Morozov (2015). "Buckling of the composite sandwich cylindrical shell with clamped ends under uniform external pressure." Composite Structures 122: 209-216.

MalekzadehFard, K., et al. (2017). "Free vibration and buckling analyses of cylindrical sandwich panel with magneto rheological fluid layer." Journal of Sandwich Structures & Materials 19(4): 397-423.

Mehralian, F. and Y. T. Beni (2016). "Size-dependent torsional buckling analysis of functionally graded cylindrical shell." Composites Part B: Engineering 94: 11-25.

Nam, V. H., et al. (2019). "Nonlinear buckling and postbuckling of sandwich FGM cylindrical shells reinforced by spiral stiffeners under torsion loads in thermal environment." Acta Mechanica 230(9): 3183-3204.

Nam, V. H. and N.-T. Trung (2019). "Buckling and postbuckling of porous cylindrical shells with functionally graded composite coating under torsion in thermal environment." Thin-Walled Structures 144: 106253.

Phuong, N. T., et al. (2019). "Nonlinear stability of sandwich functionally graded cylindrical shells with stiffeners under axial compression in thermal environment." International Journal of Structural Stability and Dynamics 19(07): 1950073.

Rahmani, M. and S. Dehghanpour (2020). "Temperature-Dependent Vibration of Various Types of Sandwich Beams with Porous FGM Layers." International Journal of Structural Stability and Dynamics: 2150016.

Rahmani, M. and Y. Mohammadi (2021). "Vibration of two types of porous FG sandwich conical shell with different boundary conditions." Structural Engineering and Mechanics 79(4): 401-413.

Rahmani, M., et al. (2019). "Vibration analysis of sandwich truncated conical shells with porous FG face sheets in various thermal surroundings." Steel and Composite Structures, An International Journal 32(2): 239-252.

Rahmani, M., et al. (2020). "Buckling analysis of different types of porous FG conical sandwich shells in various thermal surroundings." Journal of the Brazilian Society of Mechanical Sciences and Engineering 42(4): 1-16.

Rahmani, M., et al. (2019). "Buckling behavior analysis of truncated conical sandwich panel with porous FG core in different thermal conditions." Amirkabir Journal of Mechanical Engineering 52(10): 141-150.

Rahmani, M., et al. (2020). "Vibration analysis of different types of porous FG conical sandwich shells in various thermal surroundings." Journal of Applied and Computational Mechanics 6(3): 416-432.

Reddy, J. N. (2003). Mechanics of laminated composite plates and shells: theory and analysis, CRC press.

Semenyuk, N., et al. (2019). "Stability and initial post-buckling behavior of orthotropic cylindrical sandwich shells with unidirectional elastic filler." International Applied Mechanics 55(6): 636-647.

Shatov, A., et al. (2020). Buckling of composite sandwich cylindrical shell with lattice anisogrid core under hydrostatic pressure. Journal of Physics: Conference Series, IOP Publishing.

Shen, H.-S. (2003). "Postbuckling analysis of pressure-loaded functionally graded cylindrical shells in thermal environments." Engineering Structures 25(4): 487-497.

Sheng, G. and X. Wang (2018). "The dynamic stability and nonlinear vibration analysis of stiffened functionally graded cylindrical shells." Applied Mathematical Modelling 56: 389-403.

Sofiyev, A. and D. Hui (2019). "On the vibration and stability of FGM cylindrical shells under external pressures with mixed boundary conditions by using FOSDT." Thin-Walled Structures 134: 419-427.

Sofiyev, A. H., et al. (2016). "Effects of shear stresses and rotary inertia on the stability and vibration of sandwich cylindrical shells with FGM core surrounded by elastic medium." Mechanics Based Design of Structures and Machines 44(4): 384-404.

Tho Hung, V., et al. (2020). "Nonlinear buckling behavior of spiral corrugated sandwich FGM cylindrical shells surrounded by an elastic medium." Materials 13(8): 1984.

Trabelsi, S., et al. (2019). "A modified FSDT-based four nodes finite shell element for thermal buckling analysis of functionally graded plates and cylindrical shells." Engineering Structures 178: 444-459.

Vodenitcharova, T. and P. Ansourian (1996). "Buckling of circular cylindrical shells subject to uniform lateral pressure." Engineering Structures 18(8): 604-614.